Additively Manufactured Polymer Optomechanics and Their Application in Laser Systems

Fabian Kranert, Jana Budde, Moritz Hinkelmann, Roland Lachmayer, Jörg Neumann, and Dietmar Kracht

1 Introduction

In the past decade, additive manufacturing (AM) has established itself as an innovative production process in many areas of industry and research [1]. Thereby, AM can be used to create individualized parts and function-integrated systems in a single manufacturing step, which meets the requirements of new industrial demands summarized under the term "Industry 4.0" [2, 3]. Among the various polymer-based 3D printing techniques, Fused Filament Fabrication (FFF) is most prevalent, since different materials as well as printers for this process are available at low cost. It is particularly interesting for in-house fabrication, enabling components to be available at short notice [4]. Many different areas of application are now being addressed, from rapid prototyping and the manufacturing of individualized components to applications in the field of research and education. As with most AM processes, users benefit from the additional degrees of freedom in design that result from the layer-by-layer production. In addition, the use of polymers in combination with infill structures leads to lightweight components, even if the design itself was not developed with weight optimization in mind. The FFF process, in particular, also allows multi-material printing, as well as the imprinting of additional components into a structural part, which further scales the functionality [5].

F. Kranert (✉) · J. Budde · M. Hinkelmann · R. Lachmayer · J. Neumann · D. Kracht
Laser Zentrum Hannover e.V. (LZH), Hollerithallee 8, 30419 Hannover, Germany
e-mail: f.kranert@lzh.de

R. Lachmayer
Institute for Product Development, Leibniz University Hannover, An der Universität 1, 30827 Garbsen, Germany

R. Lachmayer et al. (eds.), *Generative Manufacturing of Optical, Thermal and Structural Components (GROTESK)*, https://doi.org/10.1007/978-3-030-96501-3_2

In the following chapter, we investigate the advantages of AM based on FFF to demonstrate potentials and limitations in terms of structural and thermal functionality for the production of optomechanical parts. First, the stress-free imprinting of conventional optical elements in polymer structures is presented, leading to a higher degree of integration in optomechanical systems and, at the same time, to a reduction of complexity, since additional screws or clamping elements for holding optics become redundant. Subsequently, the application potential of these simple optomechanics will be exploited by integrating the imprinted optics into additively manufactured, adjustable optomechanics and quantifying their functionality. In addition, we present manufacturing of heat sinks for mounting active optical components, such as laser crystals. Here, the imprinting of optical elements as well as sensor elements is used to advance functional integration, too. These three aspects will be combined in the end to demonstrate the applicability in a rather sophisticated optomechanic for a low-power solid-state laser system, which will be characterized in detail.

2 State of the Art

2.1 Fused Filament Fabrication

Like in most AM processes, the starting point for 3D printing a part via the FFF process is a CAD-file defining the geometric dimensions. This is converted into the STL file format, which was originally developed for stereolithography. It describes the surfaces of a solid as triangular facets and can be read by a so-called slicer, a software creating the machine code (G-code) for the printer. Therefore, the software slices the three-dimensional volume into single layers and those into the individual lines. Here, the pre-defined parameters like layer height or infill degree are considered. A more detailed explanation of these parameters follows in this section.

FFF is the most common temperature-driven extrusion method for the additive manufacturing based on polymers [6]. A schematic representation of the process is given in Fig. 1. The process is also known under the trade name Fused Deposition Modeling (FDM®) by the inventor company and by the term Fused Layer Modeling (FLM) [7]. As with any extrusion-based process, material is forced from a feedstock through a heated nozzle. In case of FFF the thermoplastic material is delivered as a filament, which is melted by electrical heating in the print head and fills a material reservoir from which the viscous polymer is extruded. The continuous, constant pressure of the subsequently fed filament forms a strand with a constant diameter and rate. By placing the strand on a building tray, i.e. a glass plate, on the building platform (x–y-plane), lines are formed, which, placed next to each other, produce two-dimensional surfaces. After completion of a layer, the build platform moves downwards and printing of the next layer is started. The stacking of several layers generates a three-dimensional structure. An important parameter

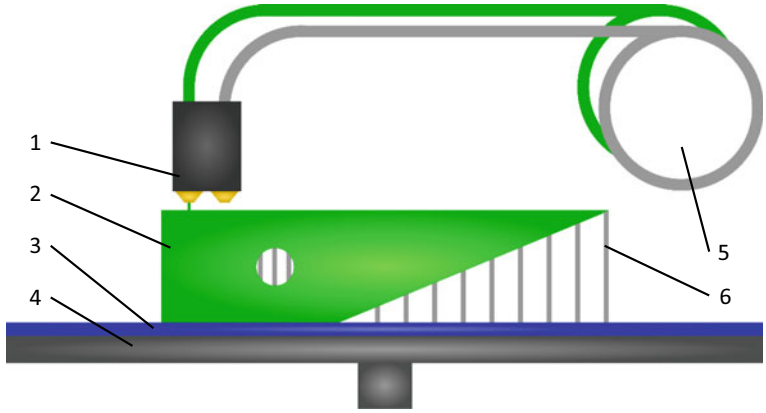

Fig. 1 Schematic illustration of the FFF process. 1: Print head with heated nozzle. 2: Generated part. 3: Build tray. 4: Build platform with retractable table. 5: Coiled filament as material stock. 6: Support structure

is the processing temperature of the material, as the polymer must be sufficiently viscous during extrusion but needs to cool quickly afterwards, to maintain the shape of the 3D printed structure [6, 8]. At the same time, the material must be warm enough when it meets the previous layer to enable a sufficient interfacial healing and achieve a solid bond between the layers. However, thermal degradation of the material must be prevented.

The nozzle in the print head defines the diameter of the extruded material strand and thus the resolution of the printing process. Consequently, it is not possible to print a feature smaller than the nozzle diameter. Thereby, a large nozzle diameter allows a higher material deposition rate, but reduces the shape fidelity compared to the digital model. The distance between nozzle and build platform or previous layer respectively, i.e. the layer height, defines the shape of the extruded strand (Fig. 2 a). Typically, this is less than or equal to half the nozzle diameter, creating an oval cross section while reducing the void space between individual lines [9, 10]. To reduce the void between the single lines further and, thus, increase the mechanical strength, they can be printed with an overlap. Same as for the nozzle diameter, a smaller layer height leads to a higher printing resolution, but a longer printing time. Usually, bodies 3D printed using FFF are not massive volumes. For sufficient structural stability, the walls, floor and ceiling are printed several layers thick, while the interior is filled with a so-called infill structure (Fig. 2b). This can be realized by different geometric patterns, for example a triangular, cubic or honeycomb structure. This infill structure as well as the infill percentage together with the shell thickness influence, among other, the mechanical stability of the 3D printed part [10]. A detailed overview of the publications that have investigated the change of different mechanical properties under variation of various parameters is presented in Popescu et al. [11]. The start and stop position of a line is always the same point. This results in a slight overlap at this

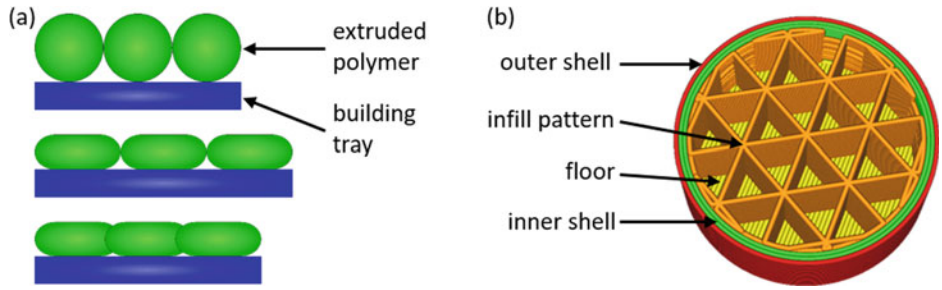

Fig. 2 **a** Illustration of the change in line cross section when the distance between the nozzle and the build platform is changed. Top: Distance equals nozzle diameter. Middle: Distance smaller than nozzle diameter. Bottom: Distance smaller than nozzle diameter with simultaneous line overlap. **b** Cross section through 3D printed cylinder. Red and green lines build the walls and represent the outer and inner shell respectively, orange lines build a triangular infill pattern and the yellow lines are the floor

point, which is visible in the case of outer lines. If the start and stop points of each layer are in the same place, a seam is formed along the z-axis. This results in a shape deviation from the CAD model along this vertical line. Either this is removed after printing, which requires a corresponding post-processing step, or a random distribution over the outer shell is created in the slicer software to minimize the influence of these points. Another factor influencing the shape fidelity is the round nozzle geometry, which generates rounded edges on outer corners [9]. The shape of the 3D printed component is also influenced by the interaction between material flow rate and axes velocity. If these are not matched, too much or too little material will be deposited in a certain area: when the print head moves at a fixed speed parallel to the x-direction and is then required to describe a right angle by transitioning the movement into the perpendicular y-direction, it will have an instantaneous speed of zero at the corner. If the extrusion volume is not zero here, excess material will be deposited.

Although the AM in general allows creating parts with a much higher design freedom than that using conventional subtractive manufacturing, limitations specific for the AM technique regarding printable structures are still given. Keeping in mind the layer-wise build-up in the FFF process it is obvious that every line needs an underlying one. Thereby, specific geometries like protruding or freestanding parts cannot be realized or only with reduced quality, since the layer will sink into the empty space underneath [6]. To avoid this, support structures are used (Fig. 1), which can be removed in a post-processing step. They can be created using either a different material than that for the actual part or the same one. In the case of a different material water-solvable polymers are often used. The benefit of these materials is evident: they can be removed easily by immerging the part into a water bath. When using the same material for part and support structure, the latter is generated to be broken off. Most slicers can generate support structures automatically.

Nevertheless, the usage of support structures always makes post-processing necessary. The exact overhang, at which the use of support structures is helpful or necessary, depends not only on the angle but also on the length of the projecting component and ranges between 45° and 75° [12–14]. At the same time, it must also be taken into account which target value is more decisive: shape accuracy or short production time with acceptance of lower surface quality and shape fidelity.

As already described, thermoplastic polymers are processed in the FFF printing. Many different polymer materials with a wide range of mechanical properties are available [11, 15]. First, FFF 3D printers were based on acrylonitrile butadiene styrene (ABS) [6, 9]. In the meantime, polylactic acid (PLA) has become a material of particular interest because, unlike many others, it can be produced from renewable raw materials and is biodegradable, non-toxic and biocompatible [16–19]. Nowadays, composite materials with added metal, stone, wood, and other particles are also commercially available and expand the application possibilities of FFF printing [16, 20–22].

Besides the above-mentioned benefits of the FFF process, two additional features are given, which are of special interest using FFF to manufacture highly integrated components. The first one is the so-called print-pause-print (PpP) scheme [5, 23]. Hereby, the printing process is paused at a specific height and an additional component, e.g. a sensor, an optical element or a previously 3D printed component is placed in a designated cutout. Afterwards, the printing process continues imprinting the component into the overall structure. This not only increases integration and functionality, but sensors also enable monitoring from within the part. The second one is the possibility to easily generate multi-material parts using a dual extrusion print head (cf. Fig. 1) and addressing different tasks of the part by tailored materials [24]. It should be noted that the use of different materials has an influence on the tensile strength of the components [25].

2.2 Printing of Optomechanical Components

AM is already present in many different areas of industry and research for a wide variety of applications. In the field of photonics, two areas have to be distinguished from each other. One is the printing of transparent and reflective optical elements for light manipulation and the other is the production of optomechanical components for mounting and adjusting optics. For the printing of optical elements, please, refer to Chap. 1 “Additive Manufacturing of Glass Materials for the Production of Optical, Thermal and Structural Components” and the relevant literature [26, 27]. The motivation for 3D printing optomechanics is driven by the cost efficiency and short-term availability, which is especially beneficial for the use in research and education. Some research groups demonstrated single optomechanics or toolboxes presenting a wide variety of components for different purposes like for example mounting or adjusting optical elements [25, 28–30].

In addition, laboratory setups for interferometry, spectroscopy or microscopy are also fabricated from such individualized toolboxes [31–35]. Next to the development of systems consisting of discrete optomechanical elements, integrated systems for a specially defined application are also demonstrated. These are systems for microscopy applications [36, 37], different kinds of spectrometry [38–41], fluorescence lifetime measurement [42], and optical scattering instrumentation [43]. For individual optomechanics, such as mirror or lens holders, commercial components are simply reprinted. In more complex systems, often only structural and, in particular, housing elements are manufactured additively. However, a higher function integration is barely addressed despite the huge potential offered by the AM approach in comparison to conventional subtractive manufacturing methods. Nevertheless, initial approaches are demonstrated to produce compact, more integrated systems. The PpP scheme is used to integrate as many of an optical system's elements as possible directly into the optomechanics, thus reducing the effort required for subsequent assembly and at the same time consistently implementing the idea of cost reduction by rendering as many commercial mechanics as possible redundant. This increase in the degree of integration of optomechanical systems through additive manufacturing is the core goal of the sGROTESK project and is demonstrated on a laser and laser amplifier system based on polymer-based additive manufacturing [44, 45]. In addition to the imprinting of optics, the embedding of additional thermal sensors for component-integrated temperature monitoring is also successfully tested here. Besides the AM based on polymers, initial preliminary work is presented to use metal-based AM processes for optomechanics [46–48]. The focus here is primarily on exploiting the several orders of magnitude higher thermal conductivity of metallic materials compared to polymers, which should enable more efficient cooling of e.g. laser crystals. The aim is also to create and take advantage of a direct bond between the optics and metal with a high heat transfer coefficient. Moreover, the higher mechanical stability of metallic materials compared to polymers is also a benefit. Although these techniques still have outstanding challenges, such as dealing with the high process temperatures required for additive processing of metallic materials, they are promising for the use in optical systems with high heat load like high-power lasers. More detailed explanations of this research can be found in Chap. 4 "Molybdenum Copper MMC for Additive Manufacturing of Thermal and Structural Components" and Chap. 5 "Additive Manufacturing of Optical, Thermal and Structural Components by Laser Metal Deposition".

3 Experiments

3.1 Printing of Single Optomechanical Components

In the following section, various 3D printed optomechanical components are presented and their functionality is quantified. Unless otherwise stated, they are printed from PLA.

Furthermore, the same commercial 3D printer (Ultimaker 3, Ultimaker) is used for all components.

3.1.1 Imprinting of optics

For the proper use of an optical element in an optical system, it must be fixed in its defined position and secured against misalignment. Usually, optics are fixed with a side-engaging screw, a retainer ring applied to the optical surface, or by other clamping mechanisms [49]. To avoid additional components such as screws and to keep the stresses introduced into the optics low, the PpP scheme, as described above, can be used for fixing the optics. Hence, the optical elements are secured directly in their respective positions in the optomechanical system. In the following, it will be examined how this imprinting affects the optical elements compared to other mounting options. For this purpose, a lens and mirror in a 3D printed holder are compared to a conventional holder from a laboratory setup in terms of induced mechanical stress and how stable the optic is seated. When designing an optomechanic, an appropriate recess for imprinting an optic needs to be considered (Fig. 3a). In addition, the described deviations between the 3D printed component and the digital model depending on the printing parameters used must be taken into account. Accordingly, the recess must be designed larger than the optical element in the lateral direction. Furthermore, the seam generated by the start and end point of the outer line of the cutout must be considered, as otherwise the insertion of the optics is more difficult and undesirable stress-generating contact points are created as described later on the basis of the measurement results shown in Fig. 5. To prevent this, an additional triangular feature is added to the round cutout (Fig. 3) where the seam is formed along the outer tip of the triangle and, thus, does not interfere further. The transition from the triangle to the circle must be rounded, to avoid the above-explained bead formation due to the inconstant print head movement in combination with the material extrusion. Since the nozzle moves close over already printed structures during the printing process, care must be taken that the components do not protrude too far to prevent a collision. This leads to problems with

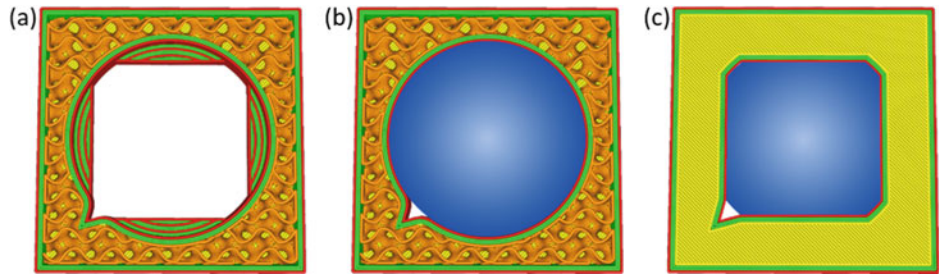

Fig. 3 Print-pause-Print scheme for the embedding of optics directly into the polymeric optomechanic. **a** The optomechanic is printed up to a defined height and the printing process is paused. **b** The optical element is inserted manually. **c** The print is continued and the optic is fixed in its position

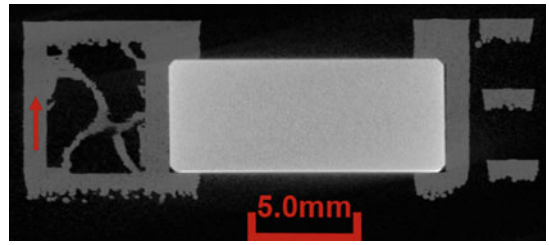

Fig. 4 X-ray image of a holder with imprinted mirror. The arrow depicts the printing direction

non-planar optics, for example the convex side of a lens. Accordingly, the design should consider the flat surface for imprinting. If this is not possible, adapters must be used. The cutout must also not be higher than the optical component, otherwise it will not be firmly secured. It was shown that protrusion of the optic by one layer height or less gives proper results for a stable and secure imprint.

As the printing material does not adhere to glass or metal surfaces, the optomechanic must be designed in a way that the printing process does not start on the inserted component but on the surrounding polymer to ensure a stable layer connection. Taking these aspects into account, form-fit imprinting of the optics is possible. To evaluate the seating of an embedded optic, tomographic images (nanotom S, GE Sensing and Inspection Technologies GmbH) of such an element were taken with a resolution of 20 μm. Figure 4 shows a cross section through a 3D printed holder with the associated 5 mm thick ½ in. fused silica mirror as an example. The polymer lines up precisely with the glass surface and no inclusions or voids are visible. Even the cavity created by the chamfer at the edge of the optic, visible on the bottom side of the optic, is closed during the imprinting process by the viscous polymer.

In addition to the X-ray image, it is also investigated whether and to what extent the imprinting of the optics introduces mechanical stress into optical elements mounted this way. Figure 5 shows the results for a stress measurement in a N-BK7 lens with a diameter of 1 in. using a polarimeter (StrainMatic M4/140, Ilis). Four different mounting cases of the lens are investigated: (a) unmounted state, (b) in a commercial mount using a retainer ring, (c) imprinted with a simple round cutout and (d) with optimized cutout (Fig. 3). Both, the commercial retainer and the plain imprinting without design optimization, result in an increased mechanical stress in the lens. Calculating the mean value of all measuring points yields a value of 0.11 MPa for the lens in the commercial holder and 0.06 MPa for the simple 3D printed holder (Fig. 5c). For the unmounted optics and the use of the improved printing design (Fig. 5d) the values are 0.04 MPa and 0.05 MPa, respectively. The same measurement is performed for a ½ in. fused silica mirror. The mirror is examined again in the unmounted state as well as after imprinting in the already optimized design. In addition, the mechanical stress is measured for the mirror being mounted in a commercial mirror holder, in which a screw clamps it laterally. In Fig. 6, the commercial holder

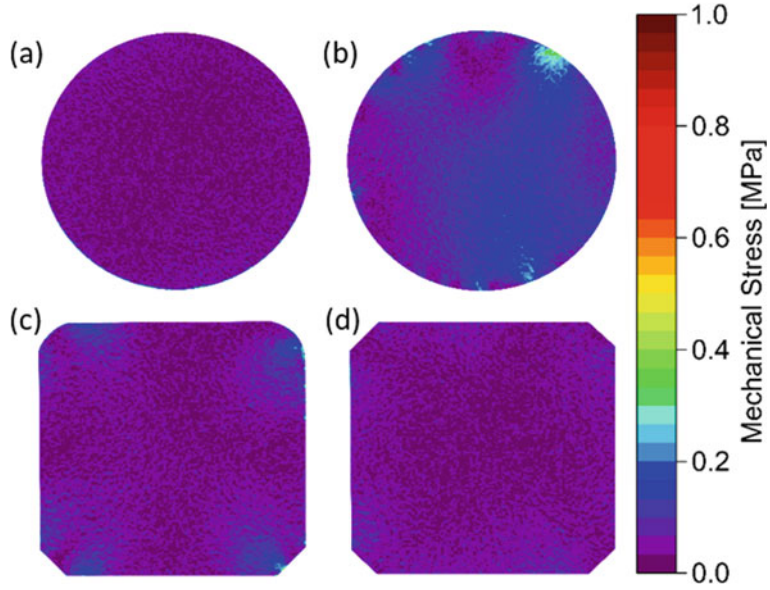

Fig. 5 Mechanical stress in a N-BK7 lens. The false color scale on the right side is valid for all graphs. **a** Unmounted. **b** Commercial holder with a retainer ring. **c** Imprinted with a simple round recess. **d** Imprinted with optimized recess, meaning the seam formation is considered

introduces stress into the optics at the points where the screw engages as well as at the two contact points of the optic in the metallic frame.

The mean stress values in the mirror are 0.04 MPa, 1.09 MPa and 0.08 MPa for being unmounted, mounted in commercial and 3D printed optomechanic, respectively. The measurements with both optics show that imprinting can reduce the mechanical stress generated compared to commercial solutions, which rely on mechanical clamping. However, even for the mirror held with the screw, the measured maximum value of 5.60 MPa is almost two orders of magnitude away from the destruction threshold for compressive loading given in the literature. Nevertheless, it must be taken into account that stress-induced birefringence in the optics already occurs at lower loads [49]. Therefore, a mounting that introduces a lower mechanical load is to be preferred.

To ensure that the optics are not less tightly fixed due to imprinting, a force is applied to the optical elements along the optical axis and at the same time it is measured whether its position changed. For the mirror fixed in the commercial holder by a screw, a force of 41 N caused the optics to slip, while the imprinted optics and the lens hold by the retainer ring did not move even at the maximum force of 50 N.

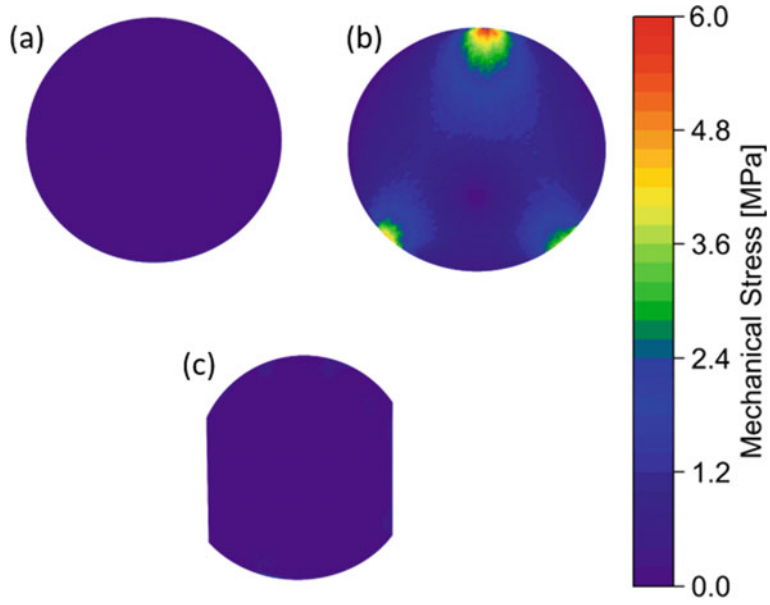

Fig. 6 Mechanical stress in fused silica mirror. The false color scale on the right side is valid for all graphs. **a** Unmounted optic. **b** Optic mounted in conventional holder. **c** Optic imprinted into PLA [28]

3.1.2 Adjustable Optomechanics

The upper sections show that an imprinting of optical elements is not only possible, but with focus on stability and induced mechanical stress beneficial. The functionality of the optomechanic is scaled by realizing adjustability, in addition to the mounting of an optical element. The use of adjustable optomechanics is crucial to enable beam alignment in an optical system. For this reason, an additively manufactured adjustable mirror mount is examined below and compared with a commercial holder. The mechanical stress was investigated for the same holder (see Fig. 6). The mechanical design in Fig. 7 consists of two individually 3D printed parts. The first, referred to below as part 1 (Fig. 7a), contains the embedded mirror, spring system and ball joint. Part 1 is printed separately from the cage system to enable the removal of the support structure, which is necessary for printing the spring system. For the part itself and the support structures the same material is used. The second part is the frame shown in Fig. 7b, referred to below as part 2. Part 1 is imprinted into part 2. The bushings for the fine thread screws are heated and inserted into the recesses provided by a proper design. The frame can also be part of a more complex optomechanic with several components imprinted. Figure 7c shows the operating principle of the kinematic holder: When the screw is turned, it moves forward and slides along the inclined surface changing the angular position of the mirror held by the spring element and ball joint. This allows the ratio of deflection angle to screw travel to be defined in the

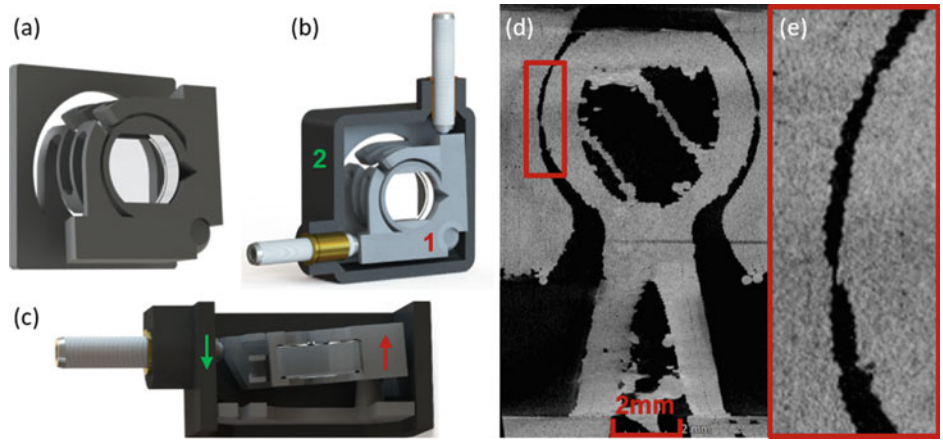

Fig. 7 **a** CAD model of mirror mount with imprinted mirror (part 1). **b** Mirror mount imprinted in frame (part 2) with fine adjuster screws and bushing. **c** Cross section of combined part with printing direction indicated. **d** Cross section through the printed ball joint. **e** Magnification by a factor of four of the area marked in red

design and adapted to different requirements. To evaluate the appearance of the printed ball joint, additional tomographic images of the holders were taken. Figure 7d shows a cross section of the 3D printed holder. An air gap between the ball and its socket is clearly visible, which is necessary to prevent the ball from sticking to its socket during printing. In the enlarged excerpt of the X-ray image, not only the step pattern from the layer-wise fabrication, but also bulges on the outer surface can be seen. Those appear, as explained, at the start and end of the outermost line of a layer. The bulges may also be contaminations from the printing process. Tests have shown that a distance of 0.25 mm between the ball and the socket in the design part reliably results in a freely movable ball joint.

The dynamic adjustment range of the 3D printed mirror mount is measured. This range is defined as the angular movement which can be realized without degeneration of performance. The initial angle is given by the design of part 1. The maximum deflection angle is defined as the angle at which the mirror returns directly to its initial position after the screw is removed. An angular range of $\pm 4°$ was aimed for, which corresponds to commercially available metal mounts. Consequently, part 1 is designed for an initial angle of $-4°$, resulting in a real initial angle of about $-3.5°$ when the fine-thread screws are in contact. With an increment of half turns, one screw is adjusted until the limits of elastic deformation are reached. During the measurement, the screw of the second axis is in contact with the holder, but its position is not changed. The maximum deflection angle is measured with 4.1°, followed by the onset of a hysteresis, i.e. the holder did not return to its initial position immediately, but with a time delay. In another experiment, the reproducibility of the positioning as well as the crosstalk between the axes is determined. Therefore,

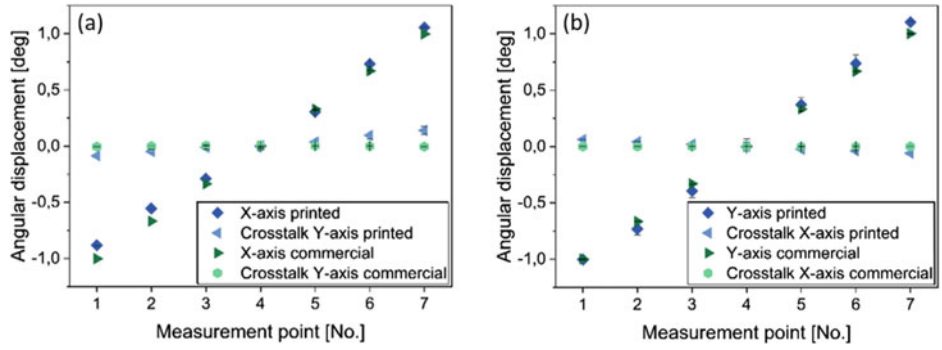

Fig. 8 Reproducibility of angular movement and crosstalk between the axes of the PLA mount compared to a commercial reference holder. **a** Displacement of the X-axis. **b** Displacement of the Y-axis [28]

the beam from a laser diode (BF-A64-0180-S5F, Sheaumann Laser, Inc.) is collimated and deflected via the mirrors onto a beam profiling camera (WinCamD-UCD12, Dataray Inc.), which returns the beam position on the camera chip. Using a 3D printed and a commercial holder (KM100, Thorlabs, Inc.), seven uniformly distributed measurement points within the range of $\pm 1°$ are approached. The measurement is performed six times with each holder. The results with the corresponding error bars are shown in Fig. 8. The first thing to note is that, like the commercial holder, the 3D printed one also shows a linear progression over the entire angular range for both axes. If the size of the error bars is considered, this gives information about the repeatability. The smaller they are, the higher the repeatability. For the metal holder and the X-axis of the 3D printed holder, these are so small that the measuring points themselves superimpose them. Quantified, the deviation for the commercial holder is less than 70 µrad for both axes and for the X-axis of the 3D printed one less than 230 µrad. However, the Y-axis of the 3D printed holder shows a significantly larger deviation of up to 1.3 mrad. An explanation for the error can be the step profile of the ball and socket described above as well as the impurities visible in Fig. 7d, which inhibit smooth gliding in the joint. The same applies to the contact surface between screw and mount. Compared to the commercial holder, a slight crosstalk of the axes can be observed, which is more pronounced for the X- than that for the Y-axis.

The long-term stability of the mirror mounts, 3D printed and commercial, is investigated by capturing the position of a deflected laser beam by the camera over 24 h with an interval of 30 s. The temperature uncertainty over a measurement period was ± 0.5 K. The angular drift for the X- and Y-axis of the commercial reference and the additively manufactured mount is depicted in Fig. 9a and b, respectively.

The metallic reference holder shows only a slight, steady drift of less than 5 µrad, which is identical for both axes. The axes of the 3D printed holder show a more pronounced shift of several 10 µrad. The measurement with this mount is performed multiple

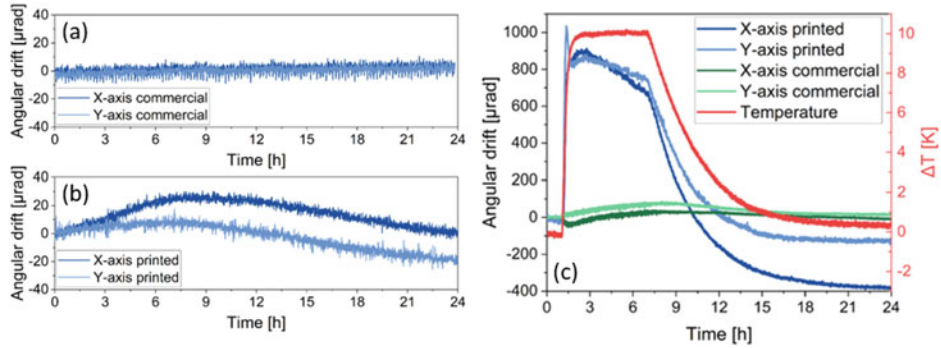

Fig. 9 Angular drift of the mount's axes over 24 h. **a** Commercial reference mount. **b** PLA mount. **c** Angular drift of the PLA and reference mount's axes under the influence of temperature change [28]

times, leading always to a drift of ≤ 100 µrad, whereas the specific profile of the drifting changes between the measurements. To ensure that the observed drift behavior is actually caused by the mirror holders, the collimated laser beam is imaged directly onto the camera chip in a further measurement. The resulting angular drift is negligibly small. The stronger drifting of the polymeric mount can be explained by the different material properties of metals and polymers. The viscoelastic properties of polymers lead to significantly stronger time-dependent effects from external influences [50].

To quantify the effect of temperature changes on the position stability of the two mounts under test, they are placed in a thermally insulated chamber, which is subjected to a temperature increase of 10 K. After a stable temperature is reached, the setup is cooled down to the initial temperature again. During the whole time the beam displacement is again captured by the beam profile camera. The test is carried out several times, leading to arbitrarily differing results, which could not be combined into a uniform scheme. Figure 9c shows a measurement in which at least the typical responses of the additive mount and the metallic reference holder to the temperature change is visible. Common to both mounts was the sudden displacement of the axes triggered by the increase in temperature. This offset reduces again with decreasing temperature. The amplitude of the displacement and the remaining offset to the initial state are varying between the different measurements. In general, the temperature increase has a significantly stronger effect on the 3D printed holder than on the commercial one. The drift of the axes is several 100 µrad up to 2 mrad for the polymer holder. In contrast, it is in the order of ≤ 100 µrad for the reference holder. Figure 9c illustrates the deflection of the 3D printed holder relative to the initial value, which is several 100 µrad. For the metallic holder, the deflection is an order of magnitude smaller. At a constant elevated temperature, a stronger drift in the axes is observed than that in the measurement at room temperature. One reason for the higher sensitivity of the polymer holder to temperature changes could be the increased influence

of temperature on material properties. For example, the coefficient of thermal expansion of the used PLA material is, compared to the aluminum-based commercial holder, about a factor of three higher.

3.1.3 Heat Sink

While optomechanics for passive optical components have been discussed so far, the following subsection will deal with active optical elements. Here, active means that there is a direct interaction with the incident light. A typical example is a laser crystal, which is excited by the absorption of pump light and emits light itself. In contrast to a passive element such as a lens, the laser crystal must not only be mounted, but generated heat must be dissipated efficiently. The main heat source in a laser crystal during the lasing process is the quantum effect, i.e. the energy difference between absorbed and emitted photons. For more detailed explanations of solid-state laser systems, and in particular of the heat generation in laser crystals and the mechanisms involved, please refer to the detailed descriptions in the relevant technical literature [51–53]. The challenge in dealing with heat generation in laser crystals, with regard to polymeric components, is that it takes place in a limited volume of often less than half a cubic centimeter, and at the same time, depending on the pump power, heating of several tens to hundreds of Kelvin can occur. At the same time, the components used are made of materials with comparably low glass transition temperatures to enable thermoplastic softening when processed by the FFF technique. For this reason, the first approach was to use a polymer, which is printable but also thermally stable. A special polyethylene terephthalate filament (PET, 3dkTOP, 3dk.berlin) is chosen, since it can be tempered after printing and is then, according to the manufacturer, mechanically stable up to 230 °C. Using this material, a holder for a laser crystal was manufactured [44]. However, it became apparent that the load limits are quickly reached here. Using a Nd:YVO_4 crystals with a dimension of $3 \times 3 \times 11$ mm^3 and an Nd doping of 0.27 at.% the temperature in the holder next to the crystal reaches up to 190 °C when pumped with a fiber-coupled laser diode (WSLX-808-008-M-H2, Wavespectrum Laser Group Limited) at a wavelength of 808 nm and an absorbed power of 2.5 W. Rapid functional degradation is to be expected when the polymer is subjected to a thermal load close or above the material´s glass transition temperature. For this reason, the approach of simply holding the crystal was discarded and a design was developed that allows for active cooling of the crystal [25]. The developed and investigated heat sink design implemented a water flow around the crystal (see Fig. 10). Here, the cooling channel is mainly designed with the requirements of the printing process in mind. Therefore, support structures should not be required, since they cannot be removed from the cooling channel afterwards. In-depth simulations how different parameters affect the interactions between the heat sink and the laser crystal can be found in Chap. 3 “Simulation of Additive Manufactured Optomechatronic Systems”. The material thickness between crystal and cooling channel is 0.8 mm. The cooling water connection is made via the M5 thread printed along with the holder. In addition, resistance temperature detectors

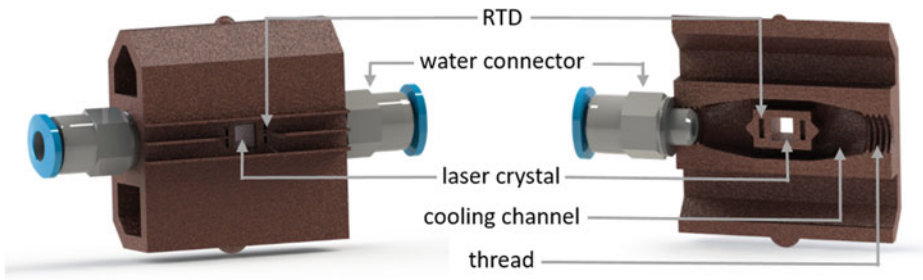

Fig. 10 CAD model of the 3D printed heat sink shown as a solid (left) and as a cross section (right). In the latter, the internal structural features are visible

(RTDs) are imprinted near the crystal at a distance of 0.8 mm, so that the temperature in the holder can be monitored. Besides the already mentioned materials PLA and PET, a third one, a copper-PLA mixture (Cu-PLA; MetalFil—Classic Copper, FormFutura) with a copper particle volume fraction of approximately 35%, is investigated for the heat sink. It is shown that the Cu-PLA material leads to the most efficient cooling, which is the reason that in the following only heat sinks 3D printed from this material are discussed [25]. Parallel to the 3D printed one, a subtractive manufactured two-part copper heat sink was tested. It is also water-cooled and serves as a reference to the printed heat sinks. An RTD is bonded to the surface of the holder to allow temperature measurement here as well. In the copper holder, the crystal is wrapped with indium foil of thickness 100 µm to optimize the contact area when clamping the crystal and thus the heat flow with the heat sink. In the case of the crystal mounted in the 3D printed heat sink, wrapping the crystal in indium foil did not show any improved heat transfer.

The interaction between the cooling water and the polymer material is investigated. For this purpose, the water absorption was determined based on the corresponding norm [54]. It is found that the water content as a mass fraction in the Cu-PLA material is only 0.2% after a storage in water for 384 h. In addition, it is tested whether the 3D printed holder remains leakage-free even when water flows through it for a longer period. After more than 210 days, no water leakage is observed. In order to evaluate the suitability of the 3D printed heat sinks in a laser system, the above described Nd:YVO_4 crystal is imprinted in the heat sink and excited with the fiber-coupled laser diode at the same wavelength and power. The temperature of the cooling water is set to 18.0 °C. The heat generation is measured via the imprinted RTD during optical pumping over 1 h and recorded at the crystal surface by a thermal imaging camera (E53, FLIR, accuracy ± 2 °C). The emissivity of the Nd:YVO_4 crystals is assumed to be 0.74 [55]. A great improvement compared to the crystal holder without water-cooling is achieved, since the temperature inside the mount drops from 190 °C to 30 °C. However, as stated in Table 1, even the Cu-PLA does not cool as efficiently as it is possible with a conventional crystal heat sink based on copper. This is to be expected since the thermal conductivity of the polymer is several orders of

Table 1 Temperature in the crystal holder and on the crystal surface

Heat sink material	Temperature holder/°C	Temperature crystal/°C
Cu-PLA	29.7 ± 0.2	40.8
Copper	18.2 ± 0.1	22.6

The temperature in the holder is averaged over one hour. The temperature at the crystal surface is measured with the thermal imaging camera. Values adopted from [25]

magnitude lower than that of copper. The literature gives a thermal conductivity of about 0.25 W/ m·K for copper-filled PLA and between 240–380 W/ m·K for copper, depending on the exact composition of the copper material [56, 57].

Comparing the temperature measured with the imprinted RTD and the one measured with the thermal camera for the Cu-PLA heat sink in Table 1, it can be seen that at the location of the RTD the temperature has already dropped noticeably compared to the crystal surface. This can be explained on the one hand by the temperature gradient between the crystal and the cooling water and on the other hand by the fact that the polymer acts as an insulator due to its low thermal conductivity. For the holder made of Cu-PLA, another measurement is carried out in which the crystal is pumped over a period of 24 h. It is found that even with this significantly longer period of use of the crystal holder, there is no reduction in the cooling power over the measurement period. In addition, no deformation could be observed on the crystal holder due to the influence of temperature. This is also not to be expected, since the glass transition temperature for this material is specified as over 60 °C. An even higher operating temperature as in the case of higher pump power seems appropriate.

3.2 Integrated Optomechanical Systems

In this section, we demonstrate the integration of stand-alone optomechanical components in a rather sophisticated and complex solid-state laser system. The corresponding optical system design is shown in Fig. 11.

It consists of a tube (blue) in which the corresponding optics for shaping the pump light and the holder for the fiber of the pump diode are imprinted. In addition, two adjustable mirror mounts for the optical resonator are embedded in the tube. The holders themselves must be printed separately, as described above, due to the spring system. The tube is designed so that the heat sinks with the laser crystal, characterized above, can be inserted. This allows examining them in the additively manufactured optomechanic (AddSys) as well as in a reference setup (RefSys) based on commercial optomechanical components for a comparative characterization. To ensure this comparability, the optics as well as their distances to each other are the same in both systems. Table 2 lists the weight of the optomechanical components 3D printed for this purpose as well as the printing time.

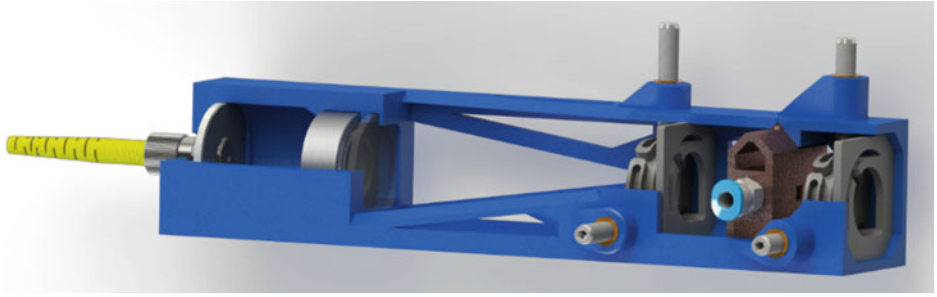

Fig. 11 CAD model of the additively manufactured optomechanic for a laser system

Table 2 List of printed optomechanics, each with material used, printing time and weight

	Material	Weight	Printing time
Tube	PLA	57 g	5 h 48 min
Mirror mount	PLA	7 g	0 h 40 min
Heat sink	Cu-PLA	21 g	2 h 36 min
Combined	–	85 g	9 h 04 min

It is worth mentioning that the laser system is not designed to reach the maximum possible optical-to-optical efficiency, since the focus is on investigating the possibilities and limitations of AM for 3D printing a laser optomechanic. In the following, three different configurations are investigated. At first, the copper heat sink is tested in the reference system, followed by the 3D printedheat sink made out of Cu-PLA. The third configuration is the 3D printed heat sink in the additively manufactured system. The laser's optical output power in the different configurations as a function of the absorbed pump power are shown in Fig. 12. In contrast to the experiments with the heat sinks in Sect. 3.1, the pump power is scaled further up the maximum output power of the pump diode of close to 9 W. The fiber of the pump diode has a core diameter of 105 µm, whereas the pump beam is collimated and focused into the laser crystal with a calculated spot size diameter of 340 µm. The cooling water for the heat sinks is set to 18.0 °C. The first resonator mirror is coated with an antireflective coating for the pump wavelength at 808 nm and a high reflective coating for the generated laser wavelength at 1064 nm. The second one, the output coupler, has a partially reflective coating for the laser wavelength with a reflectance of 91%.

The reference system has a 4% higher output power at maximum pump power when using the copper heat sink compared to using the Cu-PLA heat sink. The difference between using the additively manufactured heat sink in the reference system and the 3D printed optomechanics is marginal. For a detailed comparison, measured values for output power and optical-to-optical efficiency at maximum pump power, as well as slope

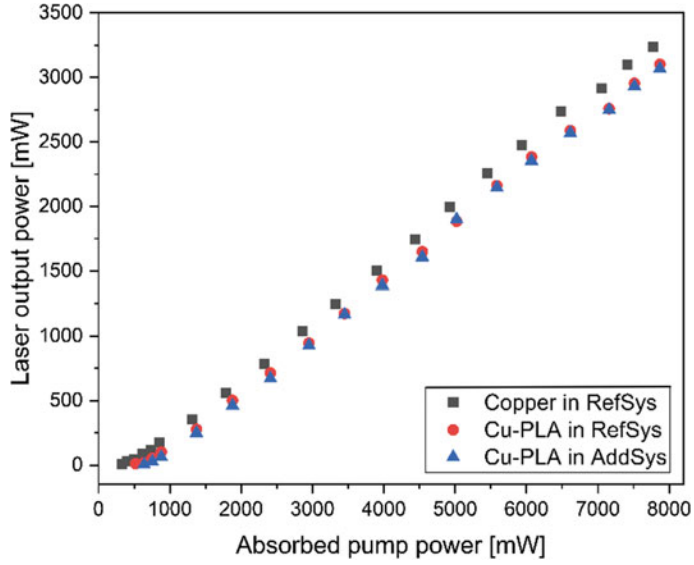

Fig. 12 Laser output power in dependence of the absorbed pump power for the copper heat sink tested in the reference system and the Cu-PLA heat sink test in both, reference and additively manufactured laser optomechanic

efficiency are listed in Table 3. In addition, the respective M^2-value is shown using a pump power of about 7 W measuring the beam diameter at five points each inside and outside the double Rayleigh length [58]. The beam pointing of the systems is determined over a period of 2 h. The value given in Table 3 describes the root mean square (rms) of all measurement points.

As described above, the differences in using the polymerheat sink in the reference system and in the additively manufactured system are negligible. This shows that the

Table 3 Overview of the parameters of the compared laser systems

System configuration	Output power / mW	Efficiency / %	Slope efficiency / %	M^2	Pointing (rms) / µrad
Copper in RefSys	3238	41.6	44.4 ± 0.3	1.36	4.53
Cu-PLA in RefSys	3101	39.4	43.0 ± 0.3	1.68	4.32
Cu-PLA in AddSys	3067	39.3	43.3 ± 0.4	1.68	5.21

The optical-to-optical efficiency is calculated at the maximum output power. The accuracy of the power values is 3.0% according to the specification of the power meter

performance of the 3D printed system, at least on short time scales, is comparable to a system based on conventional optomechanics. The slightly better performance of the laser system with the crystal in the copper heat sink can be attributed to different reasons. On the one hand, the temperature of the laser crystal has an influence on the emission cross section and, thus, on the efficiency of the laser process [59]. Furthermore, although the crystals in both holders are the same, it is not known whether they were coated in the same batch and deviations are given by the tolerance of the optical coating. In addition, the systems are adjusted manually and are therefore always subject to an individual error. In further tests, the behavior of the systems on larger time scales is investigated. The optical output power and the temperature at the heat sink are measured over a period of 10 h using a pump power of about 7 W. The results are shown in Fig. 13. Once again, the slightly higher output power of the metallic heat sink compared to the additively manufactured one is observed.

While the graphs of the output power of the Cu-PLA heat sink are almost congruent in both systems, the temperature is significantly higher when using additively manufactured optomechanics. This phenomenon will be discussed in more detail at the end of this section. In addition, the behavior of the different configurations is investigated during several on and off switching processes. For this purpose, the output power and the temperature at the heat sink are examined over 10 such cycles. Figure 14 shows for the measurements in the reference system that the output temperature remains constant over the cycles and that both temperature and output power stabilize quickly after switching on. When using the Cu-PLA heat sink in the additively manufactured system, it can be

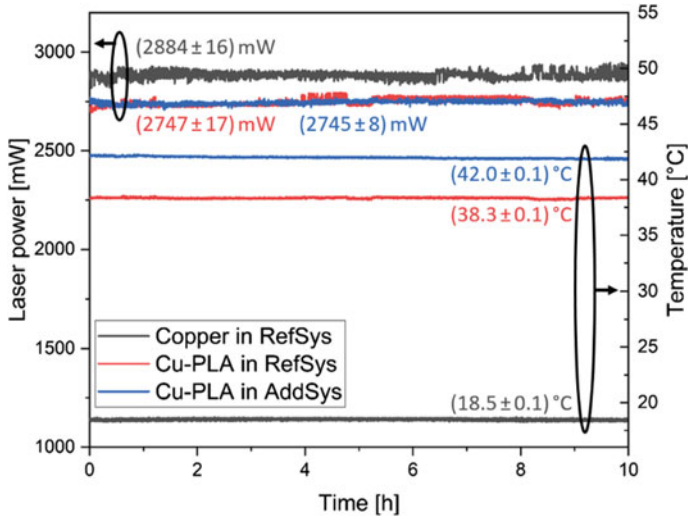

Fig. 13 Temperature measured at the heat sink and output power measured over a period of 10 h. The value in the parenthesis indicates the mean value with the associated standard deviation

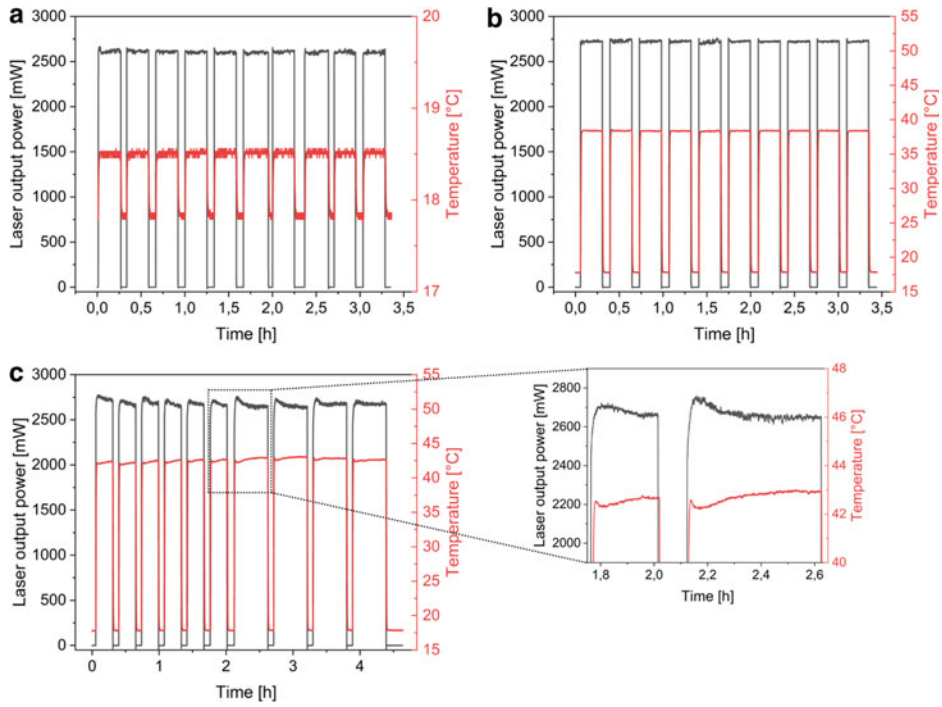

Fig. 14 Measurement of temperature and output power of the systems for 10 switching cycles. **a** Copper heat sink in reference setup. **b** Cu-PLA heat sink in reference setup. **c** Cu-PLA heat sink in additive setup

observed that longer time scales are necessary until a stable power and temperature level is reached, which is why the duration of the measurement cycles was extended. Not only the higher temperature is clearly visible again, but also the slower equilibration of the temperature accompanied by a decreasing output power.

To find a reason for the higher temperature in the additively manufactured system, a thermal imaging camera is used to take a picture of the 3D printed laser system in operation. A corresponding image is shown in Fig. 15 together with a cross section of the system‘s model. Thus, it can be determined at which points the system heats up (brighter areas in Fig. 15). The largest heat generation is on the right side, where the connection for the pump diode is located. The second place with a particularly high temperature development is between the first resonator mirror and the holder for the laser crystal. There seems to be a kind of heat accumulation, which leads to the stronger heating of the heat sink itself. This also explains the longer duration until a state of equilibrium is reached, since the temperature in the tube must stabilize in addition to the heat sink. However, it must also be said that the maximum temperature reached for the tube is 33 °C and thereby far from a critical thermal load for the PLA material.

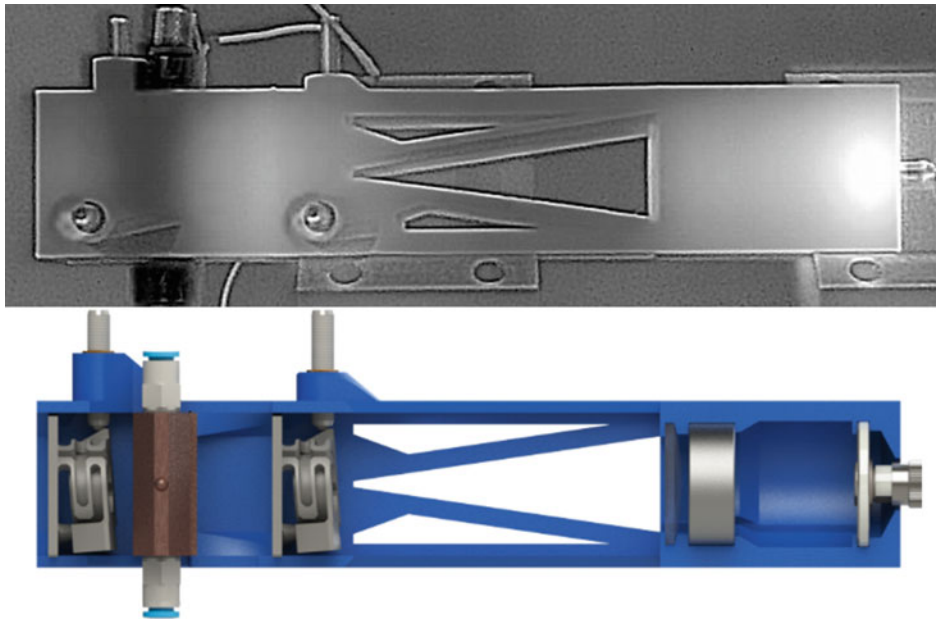

Fig. 15 Top: False color picture of the heat distribution in the laser system´s tube during operation. Brighter color corresponds to higher temperature. Bottom: Cross section of the system´s CAD model

4 Conclusion and Outlook

It has been shown that additive manufacturing based on the FFF process offers the potential for producing integrated optomechanical systems. It was thus demonstrated that optical elements can be imprinted directly into a polymer matrix, ensuring secure fixation with reduced introduction of mechanical stress. Based on this, the next innovative step to increase the level of function integration is performed by printing an adjustable optomechanic with spring system and ball joint in a single step, reducing the assembly time to a minimum. Furthermore, the possibility to manufacture water-cooled heat sinks is shown. The performance of the components is quantified by series of measurements to determine for example the stability over time or the influence of temperature changes in order to define potentials and limitations. Comparisons are also drawn with commercial and conventional components. Thereby, it was shown for the 3D printed,adjustable optomechanics that they are less stable over time and stronger influenced by temperature as the metallic one. It is quantified that polymer-based cooling performance could not be achieved to the same level as if metals were used. These points are balanced by the fact that 3D printed components can be quickly adapted to new requirements and manufactured on site, hence reducing lead-time. The elements are not only investigated

individually, but were transferred into a complex and sophisticated optomechanical system. The resulting diode-pumped solid-state laser system is compared with a conventional laboratory setup. It is shown that for low-power applications the performance of both systems is almost the same. At the same time, the 3D printed laser system benefits from a significantly reduced number of optomechanical components, as most posts and clamps become redundant. Derived from these results, the following fields of application can be defined. Since the optomechanics are highly sensitive to temperature fluctuations, it is advisable to use them in an air-conditioned environment such as a laboratory. With regard to the adjustable mirror mounts, it should be ensured that short beam paths are used in order to minimize the effect of beam drifting, which becomes particularly evident in the alignment-sensitive optical resonator. In summary, the printing of optomechanics provides the basis for cost-effective and easy-to-manufacture optomechanics. This makes such systems especially interesting for applications in the field of education or research and development, where financial resources are limited or the possibilities for manufacturing elaborately subtractive produced components are lacking. Based on the components and results presented here, a large number of other optomechanical systems can be derived and numerous applications can be addressed.

Looking at further developments, it can be said that the potential for integration has not yet been fully exploited. In order to reduce the number of single print jobs required, the next step will be to develop a system in which theheat sink for the crystal holder is also integrated with the tube for the other optics (Fig. 16).

The heat sink for the laser crystal in particular has to be redesigned, since the printing direction is different from the previous design and the cooling channel still has to be kept free of support structures. The potential of the FFF process for multi-material printing will be exploited. Furthermore, it is to be expected that the continuous progress in the field of AM, in terms of process and material development, will continuously lead to further improvements.

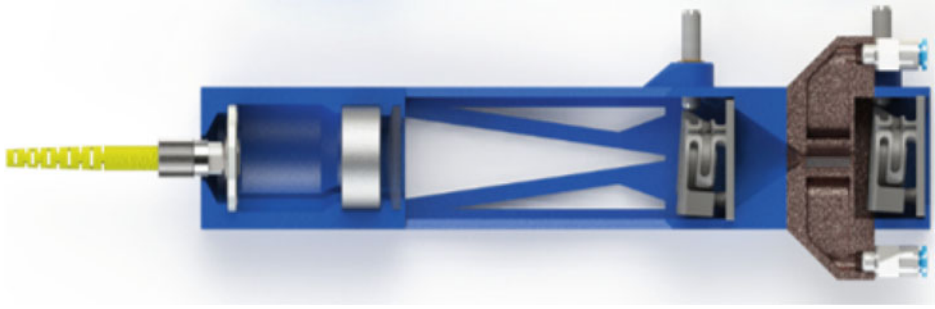

Fig. 16 Cross section of the model for an advanced additively manufactured optomechanic to scale the function integration by means of multi-material 3D printing

Acknowledgements This work was carried out within the framework of the EFRE - NBank funded project "GROTESK - Generative Manufacturing of Optical, Thermal and Structural Components" by the subproject sGROTESK (ZW6-85017815).

References

1. Haleem A., Javaid, M.: Additive manufacturing applications in industry 4.0: a review. J. Ind. Integr. Manage. **4**(4), 1930001 (2019). https://doi.org/10.1142/s2424862219300011
2. Dilberoglu, U. M., Gharehpapagh, B., Yaman, U., Dolen, M.: The role of additive manufacturing in the era of industry 4.0. Procedia Manufact **11**, 545–554 (2017). https://doi.org/10.1016/j.promfg.2017.07.148
3. Zawadzki, P., Żywicki, K.: Smart product design and production control for effective mass customization in the industry 4.0 concept. Manage Prod. Eng. Rev **7**(3), 105–112 (2016). https://doi.org/10.1515/mper-2016-0030
4. Sculpteo: The State of 3D Printing 2021 (2021)
5. Li, F., Macdonald, N.P., Guijt, R.M., Breadmore, M.C.: Increasing the functionalities of 3D printed microchemical devices by single material, multimaterial, and print-pause-print 3D printing. Lab Chip **19**(1), 35–49 (2019). https://doi.org/10.1039/c8lc00826d
6. Gibson, I., Rosen, D., Stucker, B.: Additive manufacturing technologies-rapid prototyping to direct digital manufacturing. Springer, New York (2010). ISBN: 978-1-4419-1119-3
7. VDI Gesellschaft Produktion und Logistik—VDI 3405—Additive manufacturing processes, rapid manufacturing—Basics, definitions, processes. VDI Handbuch Beuth, Berlin (2014)
8. Lepoivre, A., Boyard, N., Levy, A., Sobotka, V.: Heat transfer and adhesion study for the FFF additive manufacturing process. Procedia Manufact **47**, 948–955 (2020). https://doi.org/10.1016/j.promfg.2020.04.291
9. Gebhardt, A.: Additive Fertigungsverfahren—Additive Manufacturing und 3D-Drucken für Prototyping—Tooling—Produktion, vol. 5. Hanser Verlag GmbH + Co KG, München. ISBN: 978-3-446-44401-0
10. Akhoundi, B., Behravesh, A.H.: Effect of filling pattern on the tensile and flexural mechanical properties of FDM 3D printed products. Exp. Mech. **59**(6), 883–897 (2019). https://doi.org/10.1007/s11340-018-00467-y
11. Popescu, D., Zapciu, A., Amza, C., Baciu, F., Marinescu, R.: FDM process parameters influence over the mechanical properties of polymer specimens: a review. Polym. Testing **69**, 157–166 (2018). https://doi.org/10.1016/j.polymertesting.2018.05.020

12. Bintara, R. D., Aminnudin, A., Ida, Z., Arbianto, F., Prasetiyo, D.: The characterisitc of overhang object to material usage on FDM 3D printing technology. J. Mech. Eng. Sci. Technol. **3**(1), 35–41 (2019). https://doi.org/10.17977/um016v3i12019p035
13. Brackett, D., Ashcroft, I., Hague, R.: Topology optimization for additive manufacturing. In: 2011 International Solid Freeform Fabrication Symposium, pp. 348–362 (2011). https://doi.org/10.26153/TSW/15300
14. Mirzendehdel, A.M., Suresh, K.: Support structure constrained topology optimization for additive manufacturing. Comput. Aid. Des. **81**, 1–13 (2016). https://doi.org/10.1016/j.cad.2016.08.006
15. Roj, R., Theiß, R., Dültgen, P.: Mechanical properties of 16 different FDM-plastic types. Mater. Test. **61**(10), 999–1006 (2019). https://doi.org/10.3139/120.111413
16. Fafenrot, S., Grimmelsmann, N., Wortmann, M., Ehrmann, A.: Three-dimensional (3D) printing of polymer-metal hybrid materials by fused deposition modeling, materials **10**(10), 1199 (2017). https://doi.org/10.3390/ma10101199
17. Kuznetsov, V., Solonin, A., Urzhumtsev, O., Schilling, R., Tavitov, A.: Strength of PLA components fabricated with fused deposition technology using a desktop 3D printer as a function of geometrical parameters of the process. Polymers **10**(3), 313 (2018). https://doi.org/10.3390/polym10030313
18. Palacio, J., Orozco, V.H., López, B.L.: Effect of the molecular weight on the physicochemical properties of poly(lactic acid) nanoparticles and on the amount of ovalbumin adsorption. J. Braz. Chem. Soc. **22**(12), 2304–2311 (2011). https://doi.org/10.1590/s0103-50532011001200010
19. Afrose, F., Masood, S., Iovenitti, P., Nikzad, M., Sbarski, I.: Effects of part build orientations on fatigue behaviour of FDM-processed PLA material. Progr. Additive Manufact **1**, 21–28 (2015). https://doi.org/10.1007/s40964-015-0002-3
20. Lebedev, S.M., Gefle, O.S., Amitov, E.T., Zhuravlev, D.V., Berchuk, D.Y., Mikutskiy, E.A.: Mechanical properties of PLA-based composites for fused deposition modelling technology. Int. J. Adv. Manufact. Technol. **97**, 511–518 (2018). https://doi.org/10.1007/s00170-018-1953-6
21. Duigou, A.L., Castro, M., Bevan, R., Martin, N.: 3D printing of wood fibre biocomposites: from mechanical to actuation functionality. Mater. Des. **96**, 106–114 (2016). https://doi.org/10.1016/j.matdes.2016.02.018
22. Butt, J., Oxford, P., Sadeghi-Esfahlani, S., Ghorabian, M., Shirvani, H.: Hybrid manufacturing and mechanical characterization of Cu/PLA composites. Arab. J. Sci. Eng. **45**, 9339–9356 (2020). https://doi.org/10.1007/s13369-020-04778-y
23. Pinger, C.W., Heller, A.A., Spence, D.M.: A printed equilibrium dialysis device with integrated membranes for improved binding affinity measurements. Anal. Chem. **89**(14), 7302–7306 (2017). https://doi.org/10.1021/acs.analchem.7b01848
24. Espalin, D., Ramirez, J.A., Medina, F., Wicker, R.: Multi-material, multi-technology FDM: exploring build process variations. Rapid Prototyping J **20**(20), 236–244 (2014). https://doi.org/10.1108/rpj-12-2012-0112
25. Kranert, F., Budde, J., Hinkelmann, M., Neumann, J., Kracht, D., Lachmayer, R.: Thermische und strukturelle Analyse von Polymermaterialen in generativ gefertigten Optomechaniken für den Einsatz in der Laserentwicklung, Tagungsband 4. Niedersächsisches Symposium Materialtechnik: 25. bis 26. Februar 2021, Clausthal-Zellerfeld, virtuel (2021). https://doi.org/10.21268/20210518-5
26. Heinrich, A.: 3D-printing of optical components. Springer, Cham (2021). ISBN: 978-3-030-58959-2
27. Kloppenburg, G., Knöchelmann, M., Wolf, A.: Additive fertigung transparenter Optiken. In: Lachmayer, R., Lippert, R. B. (eds.) Additive Manufacturing Quantifiziert. Springer Vieweg Verlag, Berlin, pp. 163–174 (2017). ISBN: 978–3–662–54112–8

28. Kranert, F., Budde, J., Hinkelmann, M., Neumann, J., Kracht, D., Lachmayer, R.: 3D fabrication and characterization of polymer-imprinted optics for function-integrated, lightweight optomechanical systems. J. Laser Appl. **33**(4), 042010 (2021). https://doi.org/10.2351/7.0000492
29. Zhang, C., Anzalone, N. C., Faria, R. P., Pearce, J. M.: Open-source 3D-printable optics equipment. PLoS One **8**(3), e59840 (2013). https://doi.org/10.1371/journal.pone.0059840
30. Salazar-Serrano, L. J., Torres, J., Valencia, A.: A 3D printed toolbox for opto-mechanical components. PLoS One **12**(1), e0169832 2017, https://doi.org/10.1371/journal.pone.0169832
31. Winter, B., Shepler, D.: 3D printable optomechanical cage system with enclosure. HardwareX **3**, 62–81 (2018). https://doi.org/10.1016/j.ohx.2017.12.001
32. Gunderson, J.E., Mitchell, D.W., Bullis, R.G., Steward, J.Q., Gunderson, W.A.: Design and implementation of three-dimensional printable optomechanical components. J. Chem. Educ. **97**(10), 3673–3682 (2020). https://doi.org/10.1021/acs.jchemed.0c00631
33. Davis, E.J., Jones, M., Thiel, D.A., Pauls, S.: Using open-source, 3D printable optical hardware to enhance student learning in the instrumental analysis laboratory. J. Chem. Educ. **95**(4), 672–677 (2018). https://doi.org/10.1021/acs.jchemed.7b00480
34. Delmans, M., Haseloff, J.: μCube: a framework for 3D printable optomechanics. J. Open Hardw. **2**(1), 2 (2018). https://doi.org/10.5334/joh.8
35. Diederich, B., Lachmann, R., Carlstedt, S., Marsikova, B., Wang, H., Uwurukundo, X., Mosig, A. S., Heintzmann, R.: A versatile and customizable low-cost 3D-printed open standard for microscopic imaging. Nat. Commun. **11**, 5979 (2020). https://doi.org/10.1038/s41467-020-19447-9
36. Maia Chagas, A., Prieto-Godino, L.L., Arrenberg, A.B., Baden, T.: The €100 lab: A 3D-printable open-source platform for fluorescence microscopy, optogenetics, and accurate temperature control during behaviour of zebrafish drosophila, and caenorhabditis elegans. PLoS Biol. **15**(7), 1–21 (2017). https://doi.org/10.1371/journal.pbio.2002702
37. Nuñez, I., Matute, T., Herrera, R., Keymer, J., Marzullo, T.;, Rudge, T., Federici, F.: Low cost and open source multi-fluorescence imaging system for teaching and research in biology and bioengineering. PLoS One **12**(11), e0187163 (2017). https://doi.org/10.1371/journal.pone.0187163
38. Aydogan, O., Tasal, E.: Designing and building a 3D printed low cost modular Raman spectrometer. CERN Idea Square J. Exp. Innovation, **2**(2), 3–14 (2018). https://doi.org/10.23726/CIJ.2017.799
39. Pereira, V. R., Hosker, B. S.: Low-cost (<5€), open-source, potential alternative to commercial spectrophotometers. PLOS Biol., **17**(6), e3000321 (2019). https://doi.org/10.1371/journal.pbio.3000321
40. Porter, L. A., Chapman, C. A., Alaniz, J.A.: Simple and Iinexpensive 3D printed filter fluorometer designs: user-friendly instrument models for laboratory learning and outreach activities. J. Chem. Educ., **94**(1), 105–111 (2016). https://doi.org/10.1021/acs.jchemed.6b00495
41. Porter, L.A., Washer, B.M., Hakim, M.H., Dallinger, R.F.: User-Friendly 3D printed colorimeter models for student exploration of instrument design and performance. J. Chem. Educ. **93**(7), 1305–1309 (2016). https://doi.org/10.1021/acs.jchemed.6b00041
42. Zou, L., Mahmoud, M., Fahs, M., Liu, R., Lo, J. F.: 3D printed miniaturized spectral system for tissue fluorescence lifetime measurements. In: Proceedings SPIE, vol. 9711. Imaging, manipulation, and analysis of biomolecules, cells, and tissues IX, Article 97111S. San Francisco. https://doi.org/10.1021/acs.jchemed.6b00041
43. Nadal-Serrano, J. M., Nadal-Serrano, A., Lopez-Vallejo, M.: Democratizing science with the aid of parametric design and additive manufacturing: design and fabrication of a versatile and

low-cost optical instrument for scattering measurement. PLoS One 12(1), pp. e0187219 (2017). https://doi.org/10.1371/journal.pone.0187219
44. Kranert, F., Budde, J., Neef, P., Bernhard, R., Lammers, M., Rettschlag, K., Grabe, T., Wienke, A., Neumann, J., Wiche, H., Weslin, V., Ahlers, H., Lachmayer, R., Kracht, D.: 3D-printed, low-cost, lightweight optomechanics for a compact, low-power solid state amplifier system. In: Proceedings SPIE, vol. 11261. Components and Packaging for Laser Systems VI, Article 1126105. San Francisco, 202010.1117/12.2544268
45. Kranert, F., Budde, J., Hinkelmann, M., Wienke, A., Neumann, J., Kracht, D., Lachmayer, R.: Quasi-monolithic laser system based on 3D-printed optomechanics. In: Proceedings SPIE, vol. 11667. Components and Packaging for Laser Systems VII, Article 116670L (2021). https://doi.org/10.1117/12.2577457
46. Grabe, T., Budde, J., Kranert, F., Wienke, A., Neumann, J., Kracht, D., Lachmayer, R.: Kühlkörper-Designansatz für einen in AlSi10Mg eingebetteten YAG-Laserkristall. In: Lachmayer, R., Rettschlag, K., Kaierle, S. (eds) Konstruktion für die Additive Fertigung 2019, Springer Vieweg Verlag, Berlin, pp. 159–175 (2020). ISBN: 978-3-662-621148-7
47. Neef, P., Bernhard, R., Wiche, H., Wesling, V.: Verwendung von Kupfer-Molybdän-Pseudolegierungen für die laserbasierte additive Fertigung von Multimaterial-Verbindungen, Tagungsband 4. Niedersächsisches Symposium Materialtechnik: 25. bis 26. Februar 2021, Clausthal-Zellerfeld, virtuel, 2021, https://doi.org/10.21268/20210519-1
48. Bernhard, R., Neef, P., Wiche, H., Wesling, V., Hoff, C., Hermsdorf, J., Kaierle, S.: Additive manufacturing of copper-molybdenum pseudoalloys. In: Proceedings SPIE, vol. 11349, 3D printed optics and additive photonic Mmanufacturing II, Article 113490C. San Fransisco (2020). https://doi.org/10.1117/12.2555708
49. Yoder, P.: Mounting Optics in Optical Instruments. SPIE, Bellingham (2008). ISBN: 978-0-8194-7129-1
50. Brostow, W.: Mechanical properties. In: Mark, J. E.: Physical properties of polymers Hhandbook. Springer Science+Business Media LLC, New York, pp. 423–446 (2007). ISBN: 978-0-387-31235-4
51. Koechner, W.: Solid-State Laser Engineering. Springer Science+Business Media, New York (2006). ISBN: 978-0387-29094-2
52. Paschotta, R.: Field Guide to Lasers. SPIE, Bellingham (2008). ISBN: 978-0-8194-7826-9
53. Siegman, A.: Lasers (Revised), University Science Books, Mill Valley (1986). ISBN: 9780935702-11-8
54. DIN EN ISO 62:2008-05, Plastic. Determination of water absorption, German version
55. Newburgh, G.A., Dubinskii, M.: A high gain, composite Nd:YVO_4/SiC thin disk amplifier. In: Proceedings SPIE, vol. 9081, Laser Technology for Defense and Security X, Article 908110. Baltimore (2014). https://doi.org/10.1117/12.2053751
56. Elkholy, A., Rouby, M., Kempers, R.: Characterization of the anisotropic thermal conductivity of additively manufactured components by fused filament fabrication. Prog. Additive Manufactur. **4**, 497–515 (2019). https://doi.org/10.1007/s40964-019-00098-2
57. Bargel, H.-J., Schulze, G.: Werkstoffkunde. Springer, Berlin. ISBN: 978-3-540-79296-3 (2008)
58. Eichler, J., Dünkel, L., Eppich, B.: Die strahlqualität von lasern – wie bestimmt man beugungsmaßzahl und strahldurchmesser in der Praxis? Laser Tech. J. **1**(2), 63–66 (2004). https://doi.org/10.1002/latj.200790019
59. Délen, X., Balembois, F., Georges, P.: Temperature dependence of the emission cross section of the Nd:YVO_4 around 1064 nm and consequences on laser operation. J. Opt. Soc. Am. B **26**(5), 972–976 (2011). https://doi.org/10.1364/josab.28.000972